THE JOURNAL OF PHYSICAL CHEMISTRY C
A JOURNAL OF THE AMERICAN CHEMICAL SOCIETY

pubs.acs.org/JPCC
Article

Role of N Doping in the Reduction of Titania Nanostructures

Elena R Remesal, Ángel Morales-García,* and Francesc Illas

Cite This: J. Phys. Chem. C 2023, 127, 20128−20136
Read Online

ACCESS | Metrics & More | Article Recommendations | Supporting Information

ABSTRACT: The effect of N-doping of titania (TiO_2) nanoparticles (NPs) on their reduction through neutral O vacancy (O_{vac}) formation is investigated using all electron density functional theory-based calculations, including hybrid density functionals, and taking the bipyramidal anatase $(TiO_2)_{84}$ NP as a realistic model. The location of the N dopant is systematically analyzed, including O substitution in the $(TiO_2)_{84}$ structure and N occupying interstitial regions. Our computational study concludes that interstitial N doping is more favorable than N substituting O atoms and confirms that the presence of N reduces the energy gap. In the N-doped NP, O_{vac} formation is more favored than in undoped NP but less than in the N-doped bulk, which has important consequences.

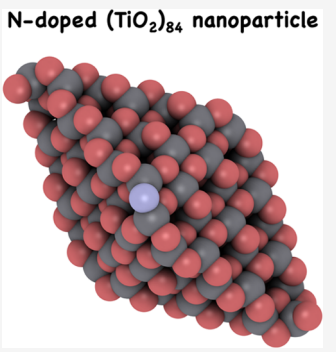

INTRODUCTION

During the last decades, an intense research activity has been carried out around semiconducting transition metal oxides (i.e., TiO_2, ZnO, WO_3) and their possible heterostructures formed by mixing configurations.[1] These materials constitute the leading families of photocatalytic materials with implications in energy and environmental science.[2,3] Since the pioneering works by Fujishima and Honda[4] and Schrauzer and Guth,[5] TiO_2 has become one of the most promising photoactive materials, especially when nanostructured, due to its intrinsic electronic properties attributed to a plentiful availability, nontoxicity, chemical stability, and high reactivity.[6] Nevertheless, TiO_2 exhibits important limitations such as a wide energy gap and fast recombination of photogenerated electrons and holes, which cause a restrictive light absorption.[7,8] These drawbacks have greatly motivated further research aimed at developing and designing TiO_2-derived materials active in the visible-light region of the electromagnetic spectrum with low recombination.[9−11]

In the last years, numerous theoretical and experimental studies on TiO_2 have been published following different strategies to overcome these drawbacks, aiming at improving the photocatalytic performance.[12−16] One of these strategies is doping stoichiometric TiO_2 polymorphs with nonmetals such as C, N, or S.[17−20] Nonmetal doping in the main has been found to be more favorable than doping with the metal counterpart due to the low rate of recombination center formation, where the photogenerated species are annihilated. Furthermore, electronic analysis confirms the presence of additional electronic states in between the valence and conduction bands of doped TiO_2 promoting the reduction of the energy gap and, consequently, the activation under visible-light illumination.[10]

Most of these investigations focused on the structural and electronic properties, and just a few of them paid attention to how nonmetal doping affects the TiO_2 reducibility through the formation of oxygen vacancies (O_{vac}). In this context, Di Valentin et al.[21] have investigated the effect of carbon impurities on the electronic band structure of bulk titania polymorphs (i.e., anatase and rutile) with respect to the oxygen partial pressure. Those results reported that the oxygen vacancy formation energy decreases up to 20% in the presence of interstitial carbon and more than 50% in the presence of substitutional carbon. This effect might be ascribed to the tendency of substitutional C atoms to accept the excess electrons generated from oxygen vacancy formation. These authors also investigated the electronic and optical properties of bulk TiO_2 modified by substitutional N.[22] From first-principles calculations, they concluded that N-doping leads to different behaviors depending on the crystalline structure. For instance, N-doping promotes red and blue shifts of the absorption edge in anatase and rutile, respectively, thus inducing different levels of photoactivity. A subsequent study aimed at characterizing the nature of paramagnetic species in N-doped TiO_2 polymorphs[23] concluded that one of the consequences of nitrogen doping is the reduction in the formation energy of an oxygen vacancy, in some cases by up to 80%. The energetically favorable charge transfer from Ti^{3+} ions to N results in a lower formation of the oxygen vacancy compared to the undoped counterpart.[24] This finding is puzzling because, as oxygen vacancy sites are efficient electron traps, it seems to indicate that N-doped titania, even exhibiting a

Received: July 11, 2023
Revised: September 7, 2023
Published: October 2, 2023

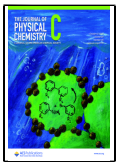

reduced gap, will easily form electron traps that are detrimental to the photocatalytic activity.

Several additional publications have characterized the effect of the dopant location on TiO_2 surfaces and nanostructures. Recently, Di Liberto et al.[25] investigated the N-doping of the exposed (001)/(101) surfaces of anatase TiO_2 heterostructures. They found that N at the (001) side of the interface constitutes the most stable doping arrangement. On the other hand, Kakil et al.[26] demonstrated that subsurface N doping in TiO_2 anatase is depth-dependent for both substitutional and interstitial N, and that N location depends on the nanocrystal facet. Moreover, they investigated N-doping of Ti_9O_{18} and $Ti_{28}O_{56}$ nanoclusters and found that the interstitial N formation energy is lower than that of substitutional N. Additional theoretical calculations predicted a decreasing of the band gap due to the presence of nitrogen, in agreement with results from UV−vis spectroscopy.[27] Combining the density functional theory (DFT) calculations and extended X-ray absorption fine structure (EXAFS) techniques, Ceotto et al.[28] studied the nitrogen location in nanocrystalline N-doped TiO_2 and concluded that, at a low concentration of N-doping, N atoms substitute O atoms, whereas at higher N-doping concentrations, oxygen vacancies appear.

A common feature of most of the previous computational studies is the use of bulk or extended surface models. However, in real nanostructured finite systems, exhibiting a variety of morphologies,[29] extended surface models represent solely their facet regions, but cannot provide information regarding other regions such as edges, corners, or apical sites, which can actively participate in the formation of the N-doped titania nanostructures as well as in the vacancy formation thereon.[30] Hence, the use of realistic nanostructure models appears necessary to account for the chemistry of these systems. The goal of the present study is precisely to analyze N-doping in TiO_2 NPs and its effect on the oxygen vacancy formation.

COMPUTATIONAL STRATEGY AND TITANIA MODELS

The realistic bipyramidal $(TiO_2)_{84}$ anatase nanoparticle (NP), well-defined in the scalable regime[30] with a Wulff-like equilibrium geometry[31] (Figure 1), has been selected to carry out a systematic exploration on N-doping and its effect on its reducibility. This NP model is representative of those found in most photocatalytic oriented experiments[29,32] that do not rely on the use of single-crystal samples with well-defined surfaces. This $(TiO_2)_{84}$ bipyramidal model exposes the most stable (101) facets, only conferring it a high structural stability. On this model, different regions are selected to generate the N-doped nanostructures. The investigated regions are located in apical (labeled as T), edge (E), facet (F), and inside (I) portions, as shown in Figure 2. Here, one needs to distinguish different O atoms as there are different atomic environments. In particular, O atoms with 2-fold (O_{2c}) and 3-fold (O_{3c}) coordination; the former are located at the shell of the bipyramid (i.e., apical, edges, and facets), while the latter are mainly located at the core of the nanoparticle. On the other hand, the interstitial dopant is located inside the channel of the structure visualized in the side view (Figures 1 and 3). Further details regarding the notations used to describe the relevant atomic environment are introduced later and clearly explained for each particular case. To inspect the stability and electronic structure of the N-doped $(TiO_2)_{84}$ NP, we perform density functional theory (DFT)-based calculations by explicitly including all electrons with the electron

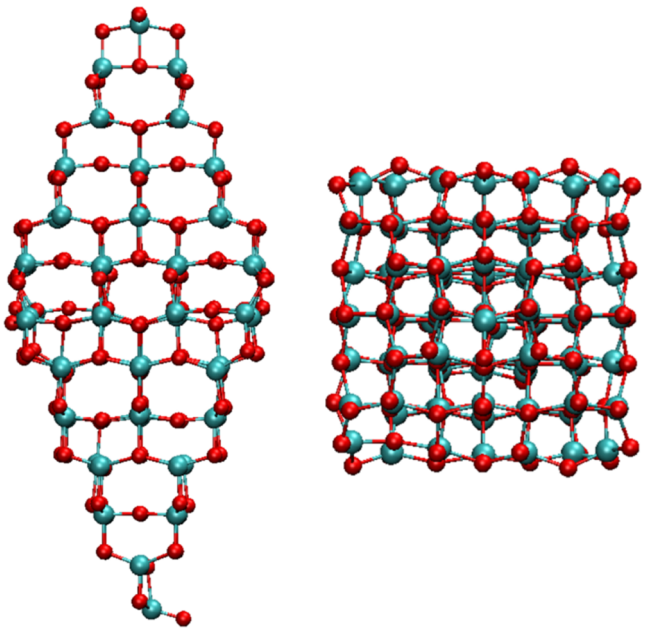

Figure 1. Side and top views of $(TiO_2)_{84}$ NP. This nanostructure exhibits a bipyramidal morphology with (101) surfaces in the eight facets. Red and cyan spheres correspond to oxygen and titanium atoms.

density described through a numerical atom-centered orbital (NAO) basis set as implemented in the Fritz Haber Institute *ab initio* molecular simulations (FHI-aims) code.[33] The Perdew−Burke−Ernzerhof (PBE)[34] density functional within the generalized gradient approximation (GGA) was selected to describe the thermodynamic stability of N-doped titania nanostructures. Calculations were carried out using the tier-1/light grid basis set. For TiO_2 systems, this setting leads to results of Gaussian type orbital (GTO) valence triple-ζ plus polarization basis set quality.[35] The convergence threshold for atomic forces in relaxation of all atoms in the N-doped and pristine $(TiO_2)_{84}$ nanostructures was set to 10^{-3} eV Å^{-1}. Due to the presence of relatively heavy Ti atoms, relativistic effects were explicitly included through the zero-order regular approach (ZORA).[36,37]

To examine the stability of N-doped TiO_2 NPs, we consider the formation energy of substitutional (N_s) and interstitial (N_i). The formation energy labeled as E_f is defined as

$$E_{f,N_s} = E_{N@Ti_{84}O_{167}} + \frac{1}{2}E_{O_2} - \frac{1}{2}E_{N_2} - E_{Ti_{84}O_{168}} \quad (1)$$

$$E_{f,N_i} = E_{N@Ti_{84}O_{168}} - \frac{1}{2}E_{N_2} - E_{Ti_{84}O_{168}} \quad (2)$$

where $E_{N@Ti_{84}O_{167}}$ and $E_{N@Ti_{84}O_{168}}$ correspond to the total energies of substitutional and interstitial doped NPs, respectively; $E_{Ti_{84}O_{168}}$ is the total energy of the undoped NP; and E_{N_2} and E_{O_2} are the total energies of the N_2 and O_2 molecules in their electronic ground state, which for the O_2 molecule is a triplet state. This definition of reference state of element is consistent with previous studies.[19,26,35] Consequently, the nitrogen molecule is taken as a convenient reference, and from the energy balance in eqs 1 and 2, we do not expect any difference when employing a different source of nitrogen. In fact, different nitrogen precursors are used in experimental studies such as ammonium hydroxide or ammonia. However, these lead to additional products, thus

https://doi.org/10.1021/acs.jpcc.3c04665
J. Phys. Chem. C 2023, 127, 20128−20136

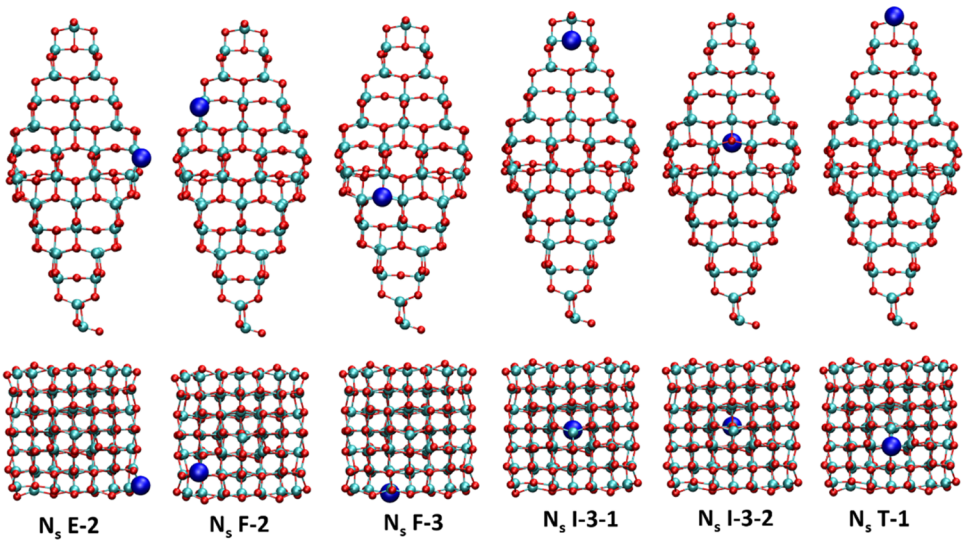

Figure 2. Side and top views of the representative optimized N_s-doped $(TiO_2)_{84}$ NPs. Cyan, red, and blue spheres denote titanium, oxygen, and nitrogen atoms, respectively. Note that the N atom has been represented by a double radius to better visualize the doping site.

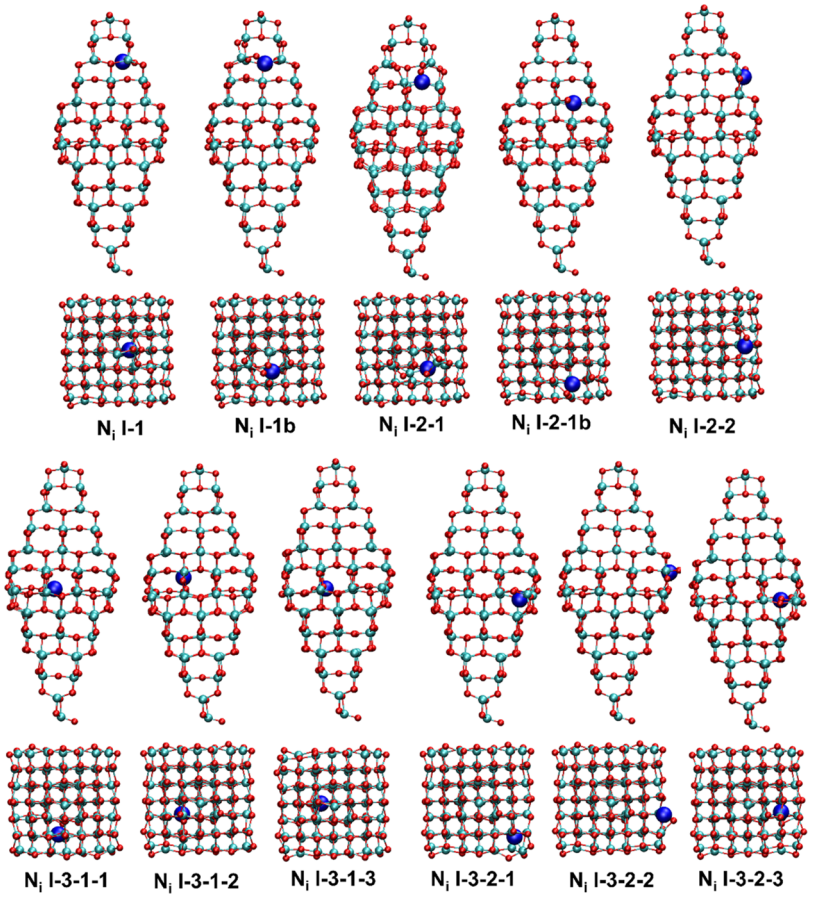

Figure 3. Side and top views of the representative optimized N_i-doped $(TiO_2)_{84}$ NPs. Note that N atoms have been represented with a double radius to better visualize the doping site. The color scheme is similar to that in Figure 2.

complicating the underlying basic chemistry, and, therefore, are not considered in the present work.

On the other hand, the oxygen vacancy formation energy E_{f,v_O} in doped titania nanostructures is defined as

$$E_{f,v_O} = E_{D@Ti_{84}O_{167}} + \frac{1}{2}E_{O_2} - E_{D@Ti_{84}O_{168}} \quad (3)$$

where $E_{D@Ti_{84}O_{168}}$ and $E_{D@Ti_{84}O_{167}}$ are the total energies of a doped $(TiO_2)_{84}$ NP, with either substitutional or interstitial N, and its reduced counterpart, respectively. In all cases, the titania nanostructures are fully relaxed. According to eq 3, $E_{f,v_O} > 0$ corresponds to the extra energy required for removing a neutral

https://doi.org/10.1021/acs.jpcc.3c04665
J. Phys. Chem. C 2023, 127, 20128−20136

single oxygen relative to the O_2 molecule; in other words, the energy required to reduce the N-doped $(TiO_2)_{84}$ NP.[38]

To analyze the electronic structure, it is necessary to recall that generalized density functionals such as PBE systematically underestimate the energy gap of semiconducting materials.[39] To overcome this deficiency, we rely on the PBEx hybrid density functional containing 12.5% of Fock exchange, which accurately reproduces the structural and electronic properties on anatase and rutile bulk titania phases.[40] Since the PBE structures for these systems are generally accurate,[41] single-point calculations with the PBEx functional are carried out at the PBE geometry. Analysis of the effect of the N atom on the energy gap relies on the Kohn−Sham energy levels of the frontier orbitals instead of density of states (DOS) plots. This is because the scrutinized systems are finite and, hence, exhibit discrete levels, and because a DOS analysis includes an artificial broadening that can somehow bias the results.

RESULTS AND DISCUSSION

Formation of N-Doped $(TiO_2)_{84}$ Nanostructures. The formation of N-doped titania nanostructures is investigated using the $(TiO_2)_{84}$ NP depicted in Figure 1 as a suitable model and analyzing O substitution by N (N_s) and interstitial N (N_i). In each case, various configurations exist, which are analyzed systematically following that recently published by some of us investigating C-doped TiO_2 NPs.[19] For N_s, six different positions in the apical (T), facet (F), edges (E), and inside (I) of the NP are investigated as highlighted in Figure 2. The formation energy of the corresponding N-doped NPs is reported in Table 1, where values are in the 4.70−5.44 eV range.

Table 1. Formation Energy of N-Doped $(TiO_2)_{84}$ NPs Calculated Following Equations 1 and 2 [a]

doping site	E_f (eV)	doping site	E_f (eV)
N_s-E-2	5.05	N_i-I-1	4.09
N_s-F-2	5.16	N_i-I-1b	2.35
N_s-F-3	4.90	N_i-I-2-1	3.20
N_s-I-3-1	4.70	N_i-I-2-2	2.62
N_s-I-3-2	5.06	N_i-I-2-1b	2.96
N_s-T-1	5.44	N_i-I-3-1-1	5.36
		N_i-I-3-1-2	3.59
		N_i-I-3-1-3	4.20
		N_i-I-3-2-1	4.15
		N_i-I-3-2-2	2.76
		N_i-I-3-2-3	4.08

[a] N_s and N_i denote substituting O by N atom and interstitial positions, respectively.

Thermodynamically speaking, the I-3-1 N-doped configuration is the one most favorable, while T-1 is the less one. These results are consistent with a previous analysis of C-doped $(TiO_2)_{84}$ NPs,[19] where the I-3-1 C-doped NP is the most stable regardless of the oxygen chemical potential.

At this point, it is interesting to compare the cases of N- and C-doping. The formation of N_s-doped titania nanostructures is energetically more favorable than the formation of C-doped ones (C_O).[19] Although there is no clear correlation between the formation energies of N- and C-doped $(TiO_2)_{84}$ NPs, the N-doped titania formation energy range is almost twice lower than that corresponding to C-doped NPs. Moreover, it is also of interest to compare our results with those involving N-doping of bulk and extended surface models. For the anatase phase, the reported N_s formation energy is ∼5 eV, independently of nitrogen concentration.[42] For the (001) and (101) anatase surfaces, the most stable position is located near the interface region, although the location on the (101) surface is thermodynamically preferred than on the (001) one.[25] In general, the present results for finite titania NPs show similar N_s formation energies to those in bulk and surface models, with values of ∼5 eV. This seems to indicate that the $(TiO_2)_{84}$ NP is large enough to mimic the facet sites of extended surfaces.

We now focus on N-doping at interstitial regions (N_i) as depicted in Figure 3. Here, the N atom localizes in one of the existing four channels (see Figure 1, side view) moving from the apical to the equatorial region. The number of sites able to accommodate the N atoms increases in the same direction, as expected from the increasing thickness at the equatorial region where the N atom finds a larger space. This is the reason why there is only one site in the apical region labeled as N_i-I-1, and three sites in the equatorial channel (N_i-I-3-2-3). All of these sites are located inside the nanoparticle and thus, only the I capital letter is used to denote them, with the three digits indicating the position with respect to the apical region in terms of proximity, the interstitial channel, and the position inside the channel, respectively. In some cases, the b letter is included in the notation to indicate that the N is near the surface of the $(TiO_2)_{84}$ NP. Table 1 lists the formation energies of N-doped titania nanostructures in the interstitial region ranking between 2.35 and 5.36 eV. The structures I-1b, I-2-2, and I-3-2-2 are the most favorable situations showing the lowest formation energies of 2.35, 2.62, and 2.76 eV, respectively. From these results, one may conclude that the N_i is energetically more favorable than N_s. Compared to a similar case of C-doping (C_i), it is clear that N_i is by far more favorable and the C_i formation energies are around 8.5 eV.[19] The comparison to the results from extended models is also interesting. There, N_i doping of the anatase bulk phase requires 4.3 eV, whereas a lower value of 3.7 eV is required to insert N_i at surface sites. Clearly, the formation of N_i-doped titania nanostructures is more favorable than either the bulk or the extended surface site, although for such extended systems N_i is also preferred to N_s.[42]

Once we have discussed the formation of N-doped $(TiO_2)_{84}$ NPs, it is important to analyze the effect that N doping has on the resulting electronic structure. To this end, we focus on the electronic structure arising from the hybrid PBEx density functional. As expected, the presence of N in the $(TiO_2)_{84}$ NP results in addition of energy levels with concomitant electronic modifications that decrease the energy gap with respect to the undoped $(TiO_2)_{84}$ NPs (see Table S1 of Supporting Information, SI). This effect has also been reported for the C-doped $(TiO_2)_{84}$ NP, but with significant differences. In general, C doping leads to a larger reduction of the energy gap. In the N-doped structures, N_s promotes a stabilization of the Kohn−Sham LUMO orbital energy relative to that of the undoped NP, resulting in the reduction of the energy gap at 1.9 eV, almost half of the value corresponding to the undoped nanostructure (3.60 eV). This trend is systematically observed except for the T-1 site, as shown in Figure 4. On the other hand, in most of the N_i-doped $(TiO_2)_{84}$ NPs, the energy gap decreases due to the addition of extra electrons, which raises the HOMO levels (Figure 5). The lowest energy gap is found for I-3-1-1 and I-3-1-2 in the equatorial cases (0.41 and 1.68 eV), whereas it is larger for the edge E-2 (1.78 eV) and inside I-3-1 and I-3-2 regions (1.88 and 1.83 eV).

https://doi.org/10.1021/acs.jpcc.3c04665
J. Phys. Chem. C 2023, 127, 20128−20136

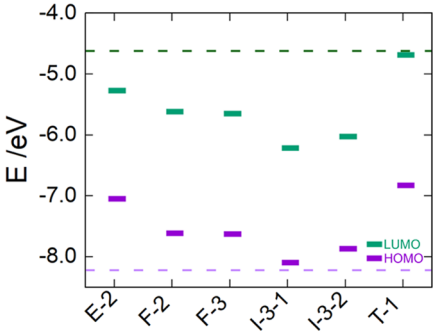

Figure 4. Kohn–Sham orbital energy level diagram of N_s-doped $(TiO_2)_{84}$ NPs obtained from DFT based calculations through the hybrid PBEx functional. The dotted lines correspond to Kohn–Sham orbital energy levels of bare $(TiO_2)_{84}$ NP.

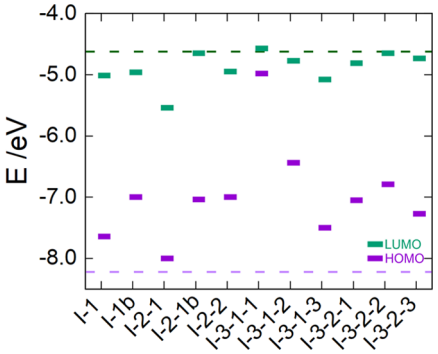

Figure 5. Kohn–Sham orbital energy level diagram of N_i-doped $(TiO_2)_{84}$ NPs obtained from DFT based calculations through the hybrid PBEx functional. The dotted lines correspond to Kohn–Sham orbital energy levels of bare $(TiO_2)_{84}$ NP.

Here, one may wonder whether the effect of the N doping is analogous (or not) to the effect of another nonmetal doping such as C. To answer this question, we extend our previous analysis[19] to investigate how doping affects the electronic structure and to make systematically the comparison between these two cases. The calculations of C-doped titania nanostructures were carried out without using spin-polarized calculations because C has an even number of electrons different from N that exposes an unpaired number as mentioned earlier. This extended analysis includes the formation of titania-doped structures by substitutional C atoms replacing O atoms, C_O, and interstitial C atoms, C_i, both having similar effects (see Figures S1 and S2). For instance, consider C_O for the I-3-2 inside, T-1 apical, and F-3 facet together with the I-1, I-2-1, I-2-2, I-3-1-1, I-3-1-3, I-3-2-1, and I-3-2-2 interstitial sites. This notation follows the same sequence described earlier when discussing N-doping at interstitial regions. In general, the LUMO energy orbital is unaltered by the presence of the C doping, but in most of the cases, the HOMO energy rises due to localized occupied states in the energy gap. These impurity states modify the absorption range, which is consistent with the experimental absorption edge shift toward the visible up to almost 1.7 eV.[43] In general, the energy gap decreases more than 2 eV with respect to $(TiO_2)_{84}$ NP by the presence of the C-doping agent. The face and apical position of C_O, F-2 and T-1, have the lowest energy gap of 0.88 and 0.83 eV, respectively, followed by the internal position, I-3-2, with 1.13 eV. This is the only case where the LUMO energy orbital is stabilized. Finally, it is necessary to point out that the largest reduction of the energy gap is observed when the C atom locates in the interstitial regions close to the equatorial area, like I-3-1-1, I-3-1-2, I-3-1-3, and I-3-2-2, whose formation energy ranges between 0.22 and 0.31 eV.

Formation of Reduced N-Doped $(TiO_2)_{84}$ Nanostructures: Formation of Oxygen Vacancies. It has been well established that the presence of certain dopants on semiconducting oxide materials favors somehow their reducibility by facilitating the generation of oxygen vacancies.[22−24] It has previously been shown that the formation of oxygen vacancies (O_{vac}) in undoped $(TiO_2)_{84}$ NP requires energies between 3.63 and 4.54 eV.[38] In that study, the NP region where vacancy creation is the most favorable is in the subsurface region. Taking advantage of our previous analysis on the bare system, we investigate here the influence of N-doping on the reducibility of the N-doped $(TiO_2)_{84}$ NP. For completeness, we also comment on the influence of C-doping on the NP reducibility.

Studying the effect of N_s doping on O_{vac} formation required fixing the N atom in one of the following sites: T-1, E-2, F-2, F-3, I-3-1, and I-3-2; then, the octahedral O atom was removed from the other sites. Therefore, for each N-doped $(TiO_2)_{84}$ NP, one has five different sites to create O_{vac}. For example, one can locate the N atom in the E-2 site and the O_{vac} can be generated in T-1, F-2, F-3, I-3-1, or I-3-2 site. An analogous strategy is followed in case of N_i doping here, fixing the N position and considering O_{vac} formation on the possible symmetry distinct sites. The results of the corresponding series of calculations are listed in Tables 2 and 3. Starting with the N_s case (Table 2), the O_{vac} formation energy ranges between 1.81 and 5.15 eV, with most cases exhibiting formation energies below 3.80 eV, thus confirming that the presence of N in the structural framework of the $(TiO_2)_{84}$ NP favors its reducibility, as found for periodic models.[22−24] More importantly, by comparing the O_{vac} formation energies of the titania nanostructures,[38] it turns out that this reduction is larger in the case of the TiO_2 NPs. To rationalize somehow this low O_{vac} energy formation in the N-doped NP, we consider the distance between the vacancy and the N dopant atom, denoted as $d_{N\text{-}Vo}$, which is also listed in Table 2. Unfortunately, there is no systematic correlation of all cases investigated, but interesting information emerges when

Table 2. Formation Energy of the Oxygen Vacancy ($E_{f,vo}$, in eV) of N_s-Doped $(TiO_2)_{84}$ NP[a]

O_{vac}	N site	$d_{N\text{-}Vo}$	$E_{f,vo}$	O_{vac}	N site	$d_{N\text{-}Vo}$	$E_{f,vo}$
E-2	F-2	11.50	2.85	I-3-1	E-2	13.16	4.33
	F-3	9.00	2.76		F-2	7.59	3.76
	I-3-1	13.06	2.93		F-3	15.42	3.84
	I-3-2	8.26	2.71		I-3-2	9.46	3.73
					T-1	3.16	5.15
F-2	E-2	11.50	3.16	I-3-2	E-2	8.33	2.24
	F-3	9.33	2.75		F-2	6.73	1.86
	I-3-1	7.47	2.73		F-3	7.92	1.96
	I-3-2	6.75	2.50		I-3-1	9.39	1.90
					T-1	12.15	3.76
F-3	E-2	9.03	3.03	T-1	E-2	14.75	3.25
	F-2	9.24	2.72		F-2	9.12	2.68
	I-3-1	15.32	2.76		F-3	17.30	2.76
	I-3-2	7.84	2.49		I-3-1	3.03	1.81
					I-3-2	12.16	2.65

[a]The O_{vac} and N notation indicates the sites in the nanoparticle where the oxygen vacancy and the N doping locates, respectively. The $d_{N\text{-}Vo}$ (in Å) corresponds to the distance between O_{vac} and N atom.

https://doi.org/10.1021/acs.jpcc.3c04665
J. Phys. Chem. C 2023, 127, 20128−20136

Table 3. Formation Energy of the Oxygen Vacancy (E_{f,v_O}, in eV) of N_i-doped $(TiO_2)_{84}$ NP[a]

O_{vac}	N site	$d_{N\text{-}Vo}$	E_{f,v_O}	O_{vac}	N site	$d_{N\text{-}Vo}$	E_{f,v_O}
E-2	I-1	10.60	3.33	I-3-2	I-1	6.78	2.25
	I-1b	9.95	3.82		I-1b	6.99	2.86
	I-2-1	8.03	3.22		I-2-1	5.74	2.40
	I-2-1b	5.22	3.66		I-2-1b	5.17	2.85
	I-2-2	4.59	3.23		I-2-2	5.97	2.11
	I-3-1-2	8.94	4.12		I-3-1-2	2.74	3.33
	I-3-2-2	3.14	4.08		I-3-2-2	6.41	2.97
F-2	I-1	6.94	3.19	I-3-1	I-1	3.15	3.63
	I-1b	4.95	3.63		I-1b	3.70	4.91
	I-2-1	5.96	3.10		I-2-1	5.10	4.30
	I-2-1b	6.26	3.61		I-2-1b	8.67	4.73
	I-2-2	10.90	3.13		I-2-2	6.98	4.09
	I-3-1-2	5.63	3.36		I-3-1-2	10.45	4.78
	I-3-2-2	11.99	3.73		I-3-2-2	11.58	4.72
F-3	I-1	13.28	3.17	T-1	I-1	5.90	2.76
	I-1b	11.97	3.65		I-1b	5.71	3.54
	I-2-1	11.04	3.13		I-2-1	7.42	2.81
	I-2-1b	7.96	3.62		I-2-1b	10.41	3.73
	I-2-2	12.26	3.08		I-2-2	9.27	3.09
	I-3-1-2	5.88	3.97		I-3-1-2	12.86	4.16
	I-3-2-2	10.07	3.73		I-3-2-2	13.66	3.76

[a]The O_{vac} and N notation indicates the sites in the nanoparticle where the oxygen vacancy and the N doping locate, respectively. The $d_{N\text{-}Vo}$ (in Å) corresponds to the distance between O_{vac} and the N atom.

analyzing each case individually. There are six cases in which the lowest E_{f,v_O} correlates with the shortest $d_{N\text{-}Vo}$ distance. Using a O_{vac}/N-atom notation to define simultaneously the position of O_{vac} and N atom, the six cases above are E-2/I-3-2, F-2/I-3-2, F-3/I-3-2, E-2/I-3-2, I-3-2/F-2, and T-1/I-3-1. In this shortlist, the E_{f,v_O} is between 1.81 and 2.71 eV. Interestingly, the inside regions are consistently involved in all of these cases. The I-3-2 site is able to hold the doping of N atom by substituting the O atom. If we spotlight on the oxygen vacancy energy formation on face (F-2, F-3) and apical (T-1) regions, we can observe a correlation between the vacancy energy formation and $d_{N\text{-}Vo}$ distance, which grows consistently as $d_{N\text{-}Vo}$ grows (see Figure 6). Compared to the undoped nanostructures, O_{vac} formation (solid lines in Figure 6) is energetically more favorable in N-doped titania nanostructures by ∼1 eV. Finally, for the N_i-doped $(TiO_2)_{84}$ NPs, Table 3 indicates a vacancy formation energy between 2.11 and 4.91 eV. As mentioned earlier, the presence of N_s favors the NP reducibility, but its presence in the interstitial region has a less effect. The most favorable situation gives formation energies of 2.11 and 2.86 eV, when the vacancy locates at the internal position (I-3-2) or apical (T-1) area. Also, the I-3-1 vacancy position is the only one that is practically unaffected by the dopant agent. Finally compared with previous studies, for the N_i cases, the presence of the dopant has less effect on reducibility than reported for the bulk, where the oxygen vacancy formation energy in the presence of N_i was around 0.6 eV.[24]

To get further insight into the nonmetal doping of TiO_2 NPs, we also performed an analogous analysis for the O_{vac} formation on the C_O and C_i doped $(TiO_2)_{84}$ NP. For this purpose, we have selected the E-2, F-2, and I-3-1 sites because these are the most stable sites for C_O doping. In addition, we also consider the I-3-2 site to directly compare with previous surface and bulk models.[17,24,26] Concerning C_i doping, we considered the I-1, I-2-2, I-3-1-2, and I-3-2-3 positions, as these are the most stable ones. For the C_O-doped NPs, we found the O_{vac} formation energy values in the 2.30−5.12 eV range (Table S2). All cases where the dopant species or oxygen vacancy is located at the I-3-2 site show an O_{vac} formation energy below 3.85 eV. This indicates that sites located in the subsurface as I-3-2 play a key role in the formation of reduced titania nanoparticles, in agreement with previous results for the undoped $(TiO_2)_{84}$ NP.[38] On the other hand, for C_i doping there is almost no effect in the oxygen vacancy energy formation, with values between 3.7 and 5.0 eV. Despite this unfavorable situation, the O_{vac} in the I-3-2 site emerges again as the most favorable thermodynamically, in consistency with the cases of C_O doping and undoped $(TiO_2)_{84}$ NPs.

Once the thermodynamic aspects have been discussed, it is necessary to describe the effect of O_{vac} on the electronic

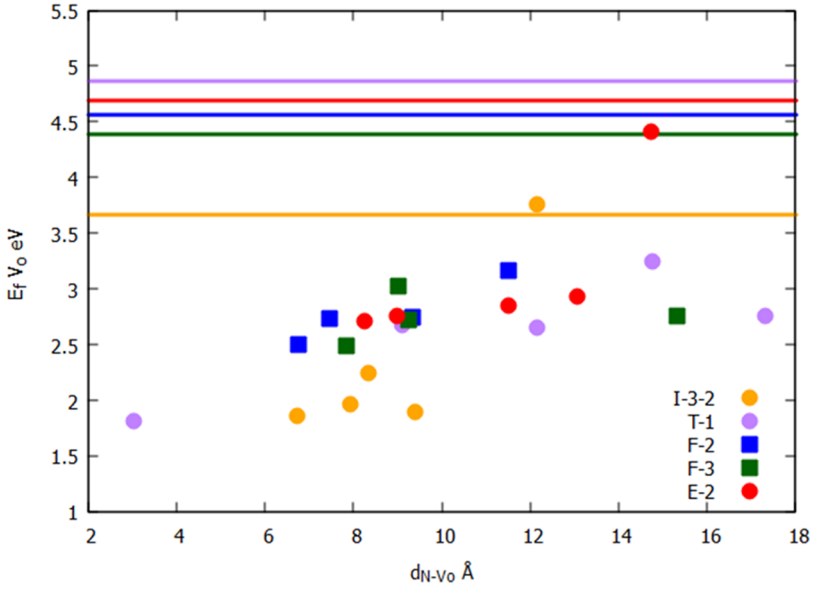

Figure 6. Trends between E_{f,v_O} and $d_{N\text{-}Vo}$. The solid lines correspond to E_{f,v_O} in bare $(TiO_2)_{84}$ NP. (See ref 38.).

https://doi.org/10.1021/acs.jpcc.3c04665
J. Phys. Chem. C 2023, 127, 20128−20136

structure of the N-doped $(TiO_2)_{84}$ NP. To make this discussion easy to follow, we focus on the cases where reducibility is facilitated in terms of lowest formation energies. At the same time, we select representative positions from the apical to the equatorial region for substituting oxygen models. For completeness, we comment on both N and C doping. We selected positions labeled as E-2, F-2, F-3, I-3-1, and I-3-2 for N_s, and E-2, F-2, I-3-1, and I-3-2 for C_O, and at least one of each channel at the interstitial models for N_i and C_i with positions I-1, I-2-2, I-3-1-2, and I-3-2-2, and I-1, I-2-2, I-3-1-2, and I-3-2-3, for N_i and C_i, respectively (see Tables S3−S6). In a previous study on the stoichiometric $(TiO_2)_{84}$ NP, it was reported that the presence of O_{vac} reduced dramatically the energy gap at ∼0.5 eV, as reproduced in Figure S3.[38] The resulting energy gap for the reduced doped $(TiO_2)_{84}$ NP is sensitive to the O_{vac} and dopant positions. When O_{vac} locates at the edges (E-2, Figure S4), the resulting energy gap of the N-doped titania nanostructure decreases by 2 eV with respect to that of undoped $(TiO_2)_{84}$ NP. This reduction is systematically observed regardless of the N position. This situation is even more pronounced in the case of C-doped $(TiO_2)_{84}$ NP, where the energy gap is reduced by 3 eV with respect to the undoped NP. Thus, C doping has a larger impact on the electronic structure of reduced/doped $(TiO_2)_{84}$ NP. A similar situation is observed when O_{vac} locates at the face (F-2, Figure S5). Here, C-doped nanostructures expose similar energy gaps (see Figure S3 for comparison). However, for the N-doped nanostructures, the energy gap decrease is larger than in the former case (Figure S5). More interesting is the case where O_{vac} locates in another facet region, labeled as F-3 (Figure S6). The energy gap decrease is analogous regardless of whether the dopant is a C or N atom and of the position they occupy. This result is similar to that where the O_{vac} is in the subsurface region (I-3-2, Figure S8). The energy gap of doped titania nanostructures shows a higher variation when creating an O_{vac} in the presence of the C atom; meanwhile, such variation is less pronounced when the titania nanostructure is N-doped.

CONCLUSIONS

The formation of N-doped titania NPs and the impact of such doping on their reducibility through a neutral oxygen vacancy formation have been computationally studied thoroughly using the bipyramidal $(TiO_2)_{84}$ NP as a realistic, representative model. For these NPs, N-doping takes place by either substituting one O atom by one N atom, or adding a N atom to the interstitial region. The former requires energies in the 4.70−5.44 eV range, with doping in the inside region being the most favored. However, interstitial doping is even more favorable as it involves formation energies in the 2.35−5.36 eV range. Interstitial N-doping is also preferred in anatase bulk but at a higher cost of 4.3 eV, and this is also the case for the anatase most stable surface, where the predicted cost is of 3.7 eV. From the electronic viewpoint, substitutional N largely stabilizes the LUMO orbital energy with a concomitant reduction of the energy gap of about 2.0 eV. Meanwhile, the most stable interstitial N doping leads to a somewhat small reduction of the energy gap going from 0.41 to 1.88 eV.

Concerning the NPs' reducibility, substitutional N leads to an oxygen vacancy formation energy in the 1.81−5.15 eV range, and in the 2.11−4.91 eV range for interstitial N. These values are sensibly larger than the 0.6 eV reported for N-doped anatase bulk. A result questioned the efficiency of N-doped titania in photocatalysis because oxygen vacancies act as efficient electron traps. Now, the fact that N doping of anatase titania nanostructures is more favorable than for anatase bulk together with the more difficult reducibility of the N-doped structure, and an additional decrease of the energy gap in the reduced N-doped $(TiO_2)_{84}$, offers a sound explanation for the observed photocatalytic efficiency of N-doped titania while showing the need for realistic models of these systems.

ASSOCIATED CONTENT

Supporting Information

The Supporting Information is available free of charge at https://pubs.acs.org/doi/10.1021/acs.jpcc.3c04665.

Listed the energy gap of (N, C)-doped $(TiO_2)_{84}$ NP using PBE and PBEx functionals (Table S1); compiles the formation energy of O_{vac} of C_O-doped and C_i-doped $(TiO_2)_{84}$ NP (Table S2); energy gap of all reduced and N_s-doped $(TiO_2)_{84}$ NPs investigated including PBE and PBEx results (Table S3); compiles the energy gap of all reduced and N_i-doped $(TiO_2)_{84}$ NPs investigated including PBE and PBEx results (Table S4); energy gap of reduced and C_O-doped $(TiO_2)_{84}$ and C_i-doped $(TiO_2)_{84}$ NPs respectively, using PBE and PBEx functionals (Tables S5 and S6); Kohn−Sham orbital energy level diagram of doped $(TiO_2)_{84}$ NPs including interstitial and substitution N or C as doped element (Figures S1−S9) (PDF)

AUTHOR INFORMATION

Corresponding Author

Ángel Morales-García − *Departament de Ciència de Materials i Química Física & Institut de Química Teòrica i Computacional (IQTCUB), Universitat de Barcelona, 08028 Barcelona, Spain;* orcid.org/0000-0003-0491-1234; Email: angel.morales@ub.edu

Authors

Elena R Remesal − *Departament de Ciència de Materials i Química Física & Institut de Química Teòrica i Computacional (IQTCUB), Universitat de Barcelona, 08028 Barcelona, Spain*

Francesc Illas − *Departament de Ciència de Materials i Química Física & Institut de Química Teòrica i Computacional (IQTCUB), Universitat de Barcelona, 08028 Barcelona, Spain;* orcid.org/0000-0003-2104-6123

Complete contact information is available at: https://pubs.acs.org/10.1021/acs.jpcc.3c04665

Author Contributions

E.R.Remesal carried out the calculations, formal analysis, data curation, and writing of a first draft. Á.M.-G. contributed to the conceptualization, supervision, funding acquisition, and writing-reviewing and editing. F.I. contributed to the funding acquisition, scientific discussion, and writing-reviewing and editing.

Notes

The authors declare no competing financial interest.

ACKNOWLEDGMENTS

The authors wish to thank Prof. Gianfranco Pacchioni for fruitful discussions relating to titania doping and reducibility. This work has benefited from the financial support from the Spanish Ministerio de Ciencia e Innovación and Agencia Estatal de Investigación (AEI) MCIN/AEI/10.13039/501100011033

through grants PID2020-115293RJ-I00, PID2021-126076NB-I00, TED2021-129506B-C22, la Unidad de Excelencia María de Maeztu CEX2021-001202-M granted to the ITQCUB, and, in part, from COST Action CA18234 and Generalitat de Catalunya 2021SGR00079 grant. The authors are indebted to the Red Española de Supercomputación (RES) for the generous allocation of computational resources.

REFERENCES

(1) Karthikeyan, C.; Arunachalam, P.; Ramachandran, K.; Al-Mayouf, A. M.; Karuppuchamy, S. Recent advances in semiconductor metal oxides with enhanced methods for solar photocatalytic applications. *J. Alloys Compd.* **2020**, *828*, No. 154281.

(2) Serpone, N.; Emeline, A. V. Semiconductor Photocatalysis−Past, Present, and Future Outlook. *J. Phys. Chem. Lett.* **2012**, *3*, 673−677.

(3) Zhang, L.; Ran, J.; Qiao, S.-Z.; Jaroniec, M. Characterization of semiconductor photocatalysts. *Chem. Soc. Rev.* **2019**, *48*, 5184−5206.

(4) Fujishima, A.; Honda, K. Electrochemical Photolysis of Water at a Semiconductor Electrode. *Nature* **1972**, *238*, 37−38.

(5) Schrauzer, G. N.; Guth, T. D. Photolysis of Water and Photoreduction of Nitrogen on Titanium Dioxide. *J. Am. Chem. Soc.* **1977**, *99*, 7189−7193.

(6) Linsebigler, A. L.; Lu, G.; Yates, J. T., Jr. Photocatalysis on TiO_2 Surfaces: Principles, Mechanisms, and Selected Results. *Chem. Rev.* **1995**, *95*, 735−758.

(7) Villa, K.; Galán-Mascarós, J. R.; López, N.; Palomares, E. Photocatalytic water splitting: advantages and challenges. *Sustainable Energy Fuels* **2021**, *5*, 4560−4569.

(8) Melchionna, M.; Fornasiero, P. Updates on the Roadmap for Photocatalysis. *ACS Catal.* **2020**, *10*, 5493−5501.

(9) Schneider, J.; Matsuoka, M.; Takeuchi, M.; Zhang, J.; Horiuchi, Y.; Anpo, M.; Bahnemann, D. W. Understanding TiO_2 Photocatalysis: Mechanisms and Materials. *Chem. Rev.* **2014**, *114*, 9919−9986.

(10) Etacheri, V.; Di Valentin, C.; Scheneider, J.; Bahnemmann, D.; Pillai, S. C. Visible-light activation of TiO_2 photocatalysts: Advances in theory and experiments. *J. Photochem. Photobiol.* **2015**, *25*, 1−29.

(11) Morales-García, Á.; Viñes, F.; Sousa, C.; Illas, F. Towards a Rigorous Theoretical Description of Photocatalysis Using Realistic Models. *J. Phys. Chem. Lett.* **2023**, *14*, 3712−3720.

(12) Asahi, R.; Morikawa, T.; Ohwaki, T.; Aoki, K.; Taga, Y. Visible-light photocatalysis in nitrogen-doped titanium oxides. *Science* **2001**, *293*, 269−271.

(13) Liu, G.; Yu, J. C.; Lu, G. Q.; Cheng, H.-M. Crystal facet engineering of semiconductor photocatalysts: motivations, advances and unique properties. *Chem. Commun.* **2011**, *47*, 6763−6783.

(14) Wang, S.; Liu, G.; Wang, L. Crystal Facet Engineering of Photoelectrodes for Photoelectrochemical Water Splitting. *Chem. Rev.* **2019**, *119*, 5192−5247.

(15) Chen, J.; Qiu, F.; Xu, W.; Cao, S.; Zhu, H. Recent progress in enhancing photocatalytic efficiency of TiO_2-based materials. *Appl. Catal., A* **2015**, *495*, 131−140.

(16) Wang, H.; Zhang, L.; Chen, Z.; Hu, J.; Li, S.; Wang, Z.; Liu, J.; Wang, X. Semiconductor heterojunction photocatalysts: design, construction, and photocatalytic performances. *Chem. Soc. Rev.* **2014**, *43*, 5234−5244.

(17) Chen, X.; Burda, C. The Electronic Origin of the Visible-Light Absorption Properties of C-. N- and S-Doped TiO_2 Nanomaterials. *J. Am. Chem. Soc.* **2008**, *130*, 5018−5019.

(18) Ohno, T.; Mitsui, T.; Matsumura, M. Photocatalytic Activity of S-Doped TiO_2 Photocatalyst under Visible Light. *Chem. Lett.* **2003**, *32*, 364−365.

(19) Remesal, E. R.; Morales-García, Á. Carbon-doped anatase titania nanoparticles: similarities and differences with respect to bulk and extended surface models. *Phys. Chem. Chem. Phys.* **2022**, *24*, 21381−21387.

(20) Wang, Y. Y.; Chem, Y. X.; Barakat, T.; Zeng, Y. J.; Liu, J.; Siffert, S.; Su, B.-L. Recent advances in non-metal doped titania for solar-driven photocatalytic/photochemical water-splitting. *J. Energy Chem.* **2022**, *66*, 529−559.

(21) Di Valentin, C.; Pacchioni, G.; Selloni, A. Theory of Carbon Doping of Titanium Dioxide. *Chem. Mater.* **2005**, *17*, 6656−6665.

(22) Di Valentin, C.; Pacchioni, G.; Selloni, A. Origin of the different photoactivity of N-doped anatase and rutile TiO_2. *Phys. Rev. B* **2004**, *70*, No. 085116.

(23) Di Valentin, C.; Pacchioni, G.; Selloni, A.; Livraghi, S.; Giamello, E. Characterization of Paramagnetic Species in N-doped TiO_2 Powders by EPR Spectroscopy and DFT Calculations. *J. Phys. Chem. B* **2005**, *109*, 11414.

(24) Livraghi, S.; Paganini, M. C.; Giamello, E.; Selloni, A.; Di Valentin, C.; Pacchioni, G. Origino f Photoactivity of Nitrogen-Doped Titanium Dioxide under Visible Light. *J. Am. Chem. Soc.* **2006**, *128*, 15666−15671.

(25) Di Liberto, G.; Tosoni, S.; Pacchioni, G. Nitrogen doping in coexposed (001)-(101) anatase TiO_2 surfaces: a DFT study. *Phys. Chem. Chem. Phys.* **2019**, *21*, 21497−21505.

(26) Kakil, S. A.; Abdullah, H. Y.; Abdullah, T. G.; Manini, N. Subsurface depth dependence of nitrogen doping in TiO_2 anatase: a DFT study. *J. Phys.: Condens. Matter* **2021**, *33*, No. 205703.

(27) Kakil, S. A.; Abdullah, H. Y.; Abdullah, T. G. Theoretical and experimental investigation of the electronic and optical properties of pure and interstitial nitrogen-doped $(TiO_2)_n$ cluster. *Opt. Quant. Electron.* **2022**, *54*, 635.

(28) Ceotto, M.; Lo Presti, L.; Cappelletti, G.; Meroni, D.; Spadavecchia, F.; Zecca, R.; Leoni, M.; Scardi, P.; Bianchi, C. L.; Ardizzone, S. About the Nitrogen Location in Nanocrystalline N-Doped TiO_2: Combined DFT and EXAFS Approach. *J. Phys. Chem. C* **2012**, *116*, 1764−1771.

(29) Cargnello, M.; Gordon, T. R.; Murray, C. B. Solution-Phase Synthesis of Titanium Dioxide Nanoparticles and Nanocrystals. *Chem. Rev.* **2014**, *114*, 9319−9345.

(30) Bromley, S. T.; Moreira, I. de P. R.; Neyman, K. M.; Illas, F. Approaching nanoscale oxides: models and theoretical methods. *Chem. Soc. Rev.* **2009**, *38*, 2657−2670.

(31) Morales-García, Á.; Escatllar, A. M.; Illas, F.; Bromley, S. T. Understanding the interplay between size, morphology and energy gap in photoactive TiO_2 nanoparticles. *Nanoscale* **2019**, *11*, 9032−9041.

(32) Mino, L.; Morales-García, Á.; Bromley, S. T.; Illas, F. Understanding the nature and location of hydroxyl groups on hydrated titania nanoparticles. *Nanoscale* **2021**, *13*, 6577−6585.

(33) Blum, V.; Gehrke, R.; Hanke, P.; Havu, P.; Havu, V.; Ren, X.; Reuter, K.; Scheffler, M. Ab initio molecular simulations with numeric atom-centered orbitals. *Comput. Phys. Commun.* **2009**, *180*, 2175−2196.

(34) Perdew, J. P.; Burke, K.; Ernzerhof, M. Generalized Gradient Approximation Made Simple. *Phys. Rev. Lett.* **1996**, *77*, 3865−3868.

(35) Lamiel-García, O.; Ko, K. C.; Lee, J. Y.; Bromley, S. T.; Illas, F. When Anatase Nanoparticles Become Bulklike: Properties of Realistic TiO_2 Nanoparticles in the 1−6 nm Size Range from All Electron relativistic Density Functional Theory Based Calculations. *J. Chem. Theory Comput.* **2017**, *13*, 1785−1793.

(36) Chang, C.; Pelissier, M.; Durand, M. Regular Two-Component Pauli-like Effective Hamiltonians in Dirac Theory. *Phys. Scr.* **1986**, *34*, 394−404.

(37) van Lenthe, E.; van Leeuwen, R.; Baerends, E. J.; Snijders, J. G. Relativistic Regular Two-Component Hamiltonians. *Int. Quantum Chem.* **1994**, *57*, 281−293.

(38) Morales-García, Á.; Lamiel-García, O.; Valero, R.; Illas, F. Properties of Single Oxygen Vacancies on a Realistic $(TiO_2)_{84}$ Nanoparticle: A Challenge for Density Functionals. *J. Phys. Chem. C* **2018**, *122*, 2413−2421.

(39) Morales-García, Á.; Valero, R.; Illas, F. An Empirical, yet Practical Way To Predict the Band Gap in Solids by Using Density Functional Band Structure Calculations. *J. Phys. Chem. C* **2017**, *121*, 18862−18866.

(40) Ko, K. C.; Lamiel-García, O.; Lee, J. Y.; Illas, F. Performance of a modified hybrid functional in the simultaneous description of

https://doi.org/10.1021/acs.jpcc.3c04665
J. Phys. Chem. C 2023, 127, 20128−20136

stoichiometric and reduced TiO_2 polymorphs. *Phys. Chem. Chem. Phys.* **2016**, *18*, 12357−12367.
(41) Morales-García, Á.; Valero, R.; Illas, F. Reliable and computationally affordable prediction of the energy gap of $(TiO_2)_n$ ($10 \leq n \leq 563$) nanoparticles from density functional theory. *Phys. Chem. Chem. Phys.* **2018**, *20*, 18907−18911.
(42) Di Valentin, C.; Finazzi, E.; Pacchioni, G.; Selloni, A.; Livraghi, S.; Paganini, M. C.; Giamello, E. N-doped TiO_2: Theory and Experiment. *Chem. Phys.* **2007**, *339*, 44−56.
(43) Sakthivel, S.; Kisch, H. Daylight Photocatalysis by Carbon-Modified Titanium Dioxide. *Angew. Chem., Int. Ed.* **2003**, *42*, 4908−4911.

https://doi.org/10.1021/acs.jpcc.3c04665
J. Phys. Chem. C 2023, 127, 20128−20136